

Cross–Time Scale Interactions and Rainfall Extreme Events in Southeastern South America for the Austral Summer. Part II: Predictive Skill

Á. G. MUÑOZ,^a L. GODDARD, S. J. MASON, AND A. W. ROBERTSON

International Research Institute for Climate and Society, The Earth Institute, Columbia University, Palisades, New York

(Manuscript received 8 October 2015, in final form 17 April 2016)

ABSTRACT


Potential and real predictive skill of the frequency of extreme rainfall in southeastern South America for the December–February season are evaluated in this paper, finding evidence indicating that mechanisms of climate variability at one time scale contribute to the predictability at another scale; that is, taking into account the interference of different potential sources of predictability at different time scales increases the predictive skill. Part I of this study suggested that a set of daily atmospheric circulation regimes, or weather types, was sensitive to these cross–time scale interferences, conducive to the occurrence of extreme rainfall events in the region, and could be used as a potential predictor. At seasonal scale, a combination of those weather types indeed tends to outperform all the other candidate predictors explored (i.e., sea surface temperature patterns, phases of the Madden–Julian oscillation, and combinations of both). Spatially averaged Kendall's τ improvements of 43% for the potential predictability and 23% for real-time predictions are attained with respect to standard models considering sea surface temperature fields alone. A new subseasonal-to-seasonal predictive methodology for extreme rainfall events is proposed based on probability forecasts of seasonal sequences of these weather types. The cross-validated real-time skill of the new probabilistic approach, as measured by the hit score and the Heidke skill score, is on the order of twice that associated with climatological values. The approach is designed to offer useful subseasonal-to-seasonal climate information to decision-makers interested not only in how many extreme events will happen in the season but also in how, when, and where those events will probably occur.

1. Introduction

Extreme events are difficult to forecast, but many locations of the world exhibit some regional predictability of seasonal amount and frequency of extreme precipitation that is still useful for decision-making. The impacts of extreme rainfall events are of key socioeconomic importance for southeast South America (SESA; Muñoz et al. 2015; Bettolli et al. 2009; Mechoso et al. 2001), especially for the rainy season. The skill of

seasonal rainfall forecasts in this part of the world benefits from the influence of sea surface temperature (SST) patterns in both the Pacific and the Atlantic (Muñoz et al. 2015; Pisciotano et al. 1994; Nogués-Paegle and Mo 1997; Diaz et al. 1998; Barros and Silvestri 2002; Grimm et al. 1998, 2000). Nonetheless, the predictive skill for the austral summer [December–February (DJF)] is considerably lower than for other seasons (Almeira and Scian 2006; Pisciotano et al. 1994), in part because of a weaker influence from El Niño–Southern Oscillation (ENSO) teleconnections and the potential interference of other ocean basins on the South Atlantic convergence zone (Cazes-Boezio et al. 2003; Barreiro and Tippmann 2008; Chan et al. 2008; Drumond and Ambrizzi 2008). Other causes involve local drivers, such as soil moisture availability and its possible influence on circulation (Grimm 2003; Grimm et al. 2007).

Muñoz et al. (2015, hereafter Part I), identified several subseasonal-to-seasonal climate drivers linked to daily circulation regimes, or “weather types” (Huth et al. 2010; Jolliffe and Philipp 2010), that are conducive to extreme

 Denotes Open Access content.

^a Current affiliation: NOAA/Geophysical Fluid Dynamics Laboratory, Princeton University, Princeton, New Jersey.

Corresponding author address: Á. G. Muñoz, NOAA/Geophysical Fluid Dynamics Laboratory, Princeton University, Princeton, NJ 08540-6649.
E-mail: angel.g.munoz@noaa.gov

DOI: 10.1175/JCLI-D-15-0699.1

rainfall events in SESA, via their imposed synoptic control on mesoscale physical mechanisms (e.g., mesoscale convective systems, extratropical cyclones, and heat and moisture transport). The frequencies and sequencing of these weather types are sensitive to cross-time scale interferences between the different climate drivers and therefore are themselves candidate predictors for extreme rainfall.

More generally, the interactions between different potential sources of predictability at different time scales should increase the predictive skill of extreme events in the region and could also increase the skill for mean rainfall values. This proposition is based on the idea that mechanisms of climate variability at one time scale contribute to predictability at another. For example, subseasonal climate drivers sometimes dominate the seasonal frequency of rainfall extreme events, even during moderate ENSO phases, and hence must be considered in order to have skillful forecasts. For concrete examples see [Part I](#) and also [Hirata and Grimm \(2016\)](#).

This idea may sound obvious, but multiple state-of-the-art dynamical and statistical climate models still lack an adequate representation of these cross-time scale interferences. Although several authors have diagnosed the impact of climate drivers at different time scales on rainfall extremes (see [Part I](#) for details), their role in forecast skill was not analyzed until recently ([Moron et al. 2012, 2015](#)). Indeed, it is expected that including additional predictors should increase the model's goodness of fit, but this is not necessarily true when evaluating forecast performance. Furthermore, it has not yet been demonstrated how many or what kind of climate drivers are necessary and sufficient to increase the predictive skill. Since the skill does not add up linearly, in part because the different climate drivers are not completely independent, it is also possible that the improvement is so small that there is very little added value.

A hypothesis used in this work is that during cross-time scale interferences it is possible to define an entangled state of the predictors; that state leads to better-quality and higher-skill information of the seasonal climate and its subseasonal characteristics than using predictive information on either time scale alone. The concept of entanglement is borrowed from quantum mechanics, referring to groups of particles or waves that interact in such a way that their states cannot be described independently, though it is possible to define a state for the system as a whole. The entanglement idea is akin to the basis of Bayesian approaches and the reduction of the sample space in conditional probability; in the present context it suggests that a better specification of the state of the system in the models (via this entanglement of predictors) must provide better forecasts.

For decades, statistical and dynamical climate models have focused on ENSO as the main, and often the only,

predictor at seasonal scale, and little work has been done on the simultaneous role of climate drivers at different time scales ([Hoskins 2013](#)). Not only do cross-time scale interferences allow the possibility of more skillful forecasts but they also facilitate delivery of information at different stages, as in the ready-set-go approach ([Goddard et al. 2014](#); [Braman et al. 2013](#)). In a multistage prediction system, seasonal and possibly longer-range time-scale forecasts provide a background signal that is successively updated as forecasts at shorter time scales become available. In today's prediction systems, this updating is not implemented seamlessly, in part because subseasonal forecasts are still under development ([WMO 2013](#)) and, with a few exceptions (see, e.g., [Vitart 2014](#); [Li and Robertson 2015](#)), lack skill for lead times longer than a couple of weeks. Considering methodologies that may advance seamless prediction systems is thus needed.

The weather type approach discussed in [Part I](#) identified several potential sources of predictability conducive to extreme rainfall events—namely, ENSO, the Atlantic meridional mode (AMM), the South Atlantic dipole (SAD), and the southern annular mode (SAM) at seasonal scale and the Madden–Julian oscillation (MJO) and the South Atlantic convergence zone (SACZ) at subseasonal scale; for details, see [Part I](#). For practical purposes of real-time prediction, particular combinations (or predictive state vectors, to use the terminology of [Part I](#)) of a representative subset of these drivers will be used here.

Since the weather types can be understood as proxies of the only physically available states of the system, they represent a sort of alphabet to describe all possible synoptic states in SESA. Particular sequences (or words) may be built from that alphabet to indicate the likely occurrence of extremes. A way to represent those sequences is through a Klee diagram ([Part I](#))—a simple matrix plot that explicitly shows the daily evolution of weather types both at subseasonal and interannual scales. In this paper, Klee diagrams are the basis to build subseasonal-to-seasonal (s2s) states as representative daily sequences of atmospheric circulation regimes.

The goal of this companion paper of [Part I](#) is to explore whether or not forecasts at one time scale can be improved by considering information from other time scales. The research analyzes the associated predictive skill in the context of extreme rainfall seasonal forecasts for SESA (i.e., seasonal forecasts of weather statistics) and explores some of its consequences at shorter time scales through the use of a new methodology to produce subseasonal-to-seasonal extreme rainfall scenarios (i.e., probable intraseasonal evolution of weather statistics). The word “scenario” is used here because these are not traditional forecasts but a description of what could happen on the coming 3-month season in terms of

extreme rainfall distributions; these have nothing to do with climate change scenarios.

The paper is organized as follows: The next section describes the datasets and summarizes the methods; then the potential and real-time seasonal predictive skill of frequency of extremely wet days are studied in [section 3](#), using both empirical and dynamical ([Mason and Baddour 2008](#)) subseasonal-to-seasonal predictors. Since it is important for decision-makers to know not just the total amount of (extreme) precipitation or the frequency of (extremely) wet days but also the probable temporal distribution of these days along the target period, the new forecast methodology using s2s states is discussed in [section 4](#). The reader interested in a few concrete practical aspects of the experimental forecast system described in this paper should refer to [section 5](#). The concluding remarks are presented in [section 6](#).

2. Data and methodologies

This section summarizes information about the datasets and methods used in the study. To assess potential predictability, statistical models are built using observed candidate predictors that are synchronized with the predictand, similar to a perfect prognosis approach. Real-time predictability is evaluated through model output statistics (MOS) of dynamical model output, using simultaneous and lagged predictors as indicated in the following subsections.

a. Datasets

This study uses SST fields, the phases of MJO, and the frequency of occurrence of a set of weather types as candidate predictors. Observations and dynamical model output are considered when analyzing the predictive skill. The observations involve SST fields, MJO phases, and weather type frequencies for DJF. The dynamical forecast data involve SST field for DJF, 32-day forecasts of MJO phases (started on 13 November; see details below), and weather type frequencies for DJF.

Observed datasets are the same as in [Part I](#); the Extended Reconstructed SST, version 3b, (2° grid; [Smith et al. 2008](#)) is used for sea surface temperatures on the domain defined by 43°N – 60°S and 128° – 20°E , while the phases of the real-time multivariate MJO modes ([Wheeler and Hendon 2004](#))—RMM1 and RMM2—are directly available from the Centre for Australian Weather and Climate Research.¹ The set of six weather types are those studied in [Part I](#), computed using a

k-means analysis of the NCEP–NCAR reanalysis project, version 2 (NNRPv2; [Kalnay et al. 1996](#); [Kistler et al. 1999](#)), for geopotential height anomaly at 850 hPa. To assess the maximum potential skill, all available 28 DJF seasons for the 1982–2010 period are considered. Hereafter, the datasets described in this paragraph are referred to as “observations.”

Hindcasts, or retrospective forecasts, produced with October’s initialization of the Climate Forecast System, version 2 (CFSv2; [Saha et al. 2014](#)), are used for SST fields and to compute the CFSv2’s realizations of the observed set of weather types mentioned above. The CFSv2 forecasts are available at monthly and daily temporal resolutions (SST and geopotential height anomalies, respectively) and at 0.937° spatial resolution ([Saha et al. 2014](#)). The methodology is the same one explained in [Part I](#), and no projection is performed onto the observed weather types. Before performing the *k*-means analysis, 10 ensemble members are concatenated (the use of ensemble means from daily data tends to produce spurious weather types).

The European Centre for Medium-Range Weather Forecasts (ECMWF) MJO ensemble forecast ([Vitart 2014](#)) is used here for predictions of the MJO phases (typically, ECMWF MJO forecasts are skillful up to about one month, compared to around two weeks for CFSv2). The five-member ensemble of 32-day integrations involves a sophisticated coupled model at approximately 1° grid resolution ([Vitart 2014](#)), whose MJO predictions have improved dramatically since 2002, with an average gain of about 1 day of prediction skill per year (i.e., the system is now capable of providing skillful MJO forecasts for the next 32 days, compared to skillful forecasts for about two weeks in 2002). The forecast MJO phases are computed from the two leading principal components (PCs) provided by the ECMWF forecast for this research. The hindcasts start in 1994.

To have a common period of forecasts for the dynamical model output, and for consistency with the constraints of a real-time prediction system (see [section 5](#)), only the products that are available in mid-November are used for both CFSv2 [initialized in October; see [Saha and Tripp \(2011\)](#) for details] and ECMWF forecast (available on 13 November) for the 16 DJF seasons of the 1994–2010 period. As indicated above, the CFSv2 SST forecasts and geopotential height anomalies at 850 hPa correspond to the DJF season.

In all experiments reported here, the predictand corresponds to the observed frequency of days with rainfall amounts exceeding the 95th percentile (dR95p), using the NOAA–NCEP–CPC unified precipitation gridded dataset (1° grid; [Chen et al. 2008](#)) for the SESA domain (36° – 25.5°S , 65° – 53.5°W), and considering daily values

¹ See <http://www.bom.gov.au/climate/mjo/graphics/rmm.74toRealtime.txt>.

of all DJF seasons. The frequency of extreme events is used instead of intensity or rainfall amount because of its higher predictability (see [Part I](#)).

b. Methodologies

Although the predictions of future conditions at different time scales exhibit some common features, different methodologies are used to evaluate the predictive skill of seasonal forecasts and s2s scenarios. Unless otherwise indicated, anomalies are always computed with respect to the long-term mean of the period under consideration, and tests for statistical significance are performed using a resampling method (1000 times).

1) SEASONAL FORECASTS

In this study, seasonal forecasts are produced using canonical correlation analysis (CCA). This is a multivariate statistical method commonly used by the climate forecasting community ([Mason and Baddour 2008](#)) that calculates linear combinations of a set of candidate predictors and predictands, identifying pairs of combinations (i.e., canonical variates or modes) such that the correlations between their time series are maximized. An empirical orthogonal function (EOF) prefiltering is performed before conducting the CCA. The method permits the identification of the actual predictors from the set of candidate predictors (which do not need to be independent a priori); the canonical modes describe the preferred coupled spatial patterns relating predictors and predictands and are presumed to be physically meaningful. In this study, CCA is conducted using IRI's climate predictability tool (CPT), version 15.3.7 ([Mason and Tippet 2016](#)), which first performs supervised modal truncation of the candidate predictors and the predictand. CPT provides information that diagnoses the underlying coupled patterns and also cross-validated forecast skill metrics that allow the assessment of the associated predictability.

Deterministic cross-validated forecasts were computed for the frequency of DJF days with rainfall exceeding the 95th percentile. Since the frequency of extreme rainfall in the region does not exhibit a Gaussian distribution, it was transformed using a quantile mapping of the empirical distribution before building the models. For CCA models that use a combination of different types of predictors (e.g., SST and MJO), the modes were computed using the variance-covariance matrix after a unitary variance normalization was performed.

To avoid artificial skill, CPT verifies the skill of the resulting predictions using cross validation ([Barnston and Van den Dool 1993](#)). Here, a cross-validation window of 5 years is used, meaning that the central year of

the 5-yr window held out from the time series is predicted and the forecast is then compared to the observed values, as a simulated independent case outside of the training sample (e.g., [Barnston and Van den Dool 1993](#); [Jolliffe and Stephenson 2012](#); [Mason and Stephenson 2008](#)). This process is repeated such that each year in the dataset is forecast after reapplying the fitting algorithm for each iteration of the process, and with the climatological data redefined each time a new cross-validation window is withheld. After processing all years, the mean values of the skill metrics are provided.

The following metrics are used to evaluate the cross-validated skill of the deterministic forecasts: Kendall's τ , Spearman correlation coefficient, and the area of relative operating characteristics (ROC; [Jolliffe and Stephenson 2012](#); [Mason and Stephenson 2008](#)). Additional details are discussed in [section 3](#). Spatial maps of these metrics were produced using CPT.

A summary of the forecast methodology is presented in [Fig. 1](#). [Part I](#) determined a set of predictive state vectors or candidate predictors that could be used to forecast extreme rainfall in SESA for the DJF season. The present paper deals with forecast methodologies that could be easily put to work in national weather services of developing countries, where computational resources or highly trained personnel may be scarce. Since not all of the candidate predictors suggested in [Part I](#) are currently available operationally, the predictive skill is evaluated here using the following list of candidate predictors:

- (i) SST, the PCs of the first eight EOFs of the SST field for the domain defined by 43°N–60°S, 128°–20°E;
- (ii) MJO, the frequency of occurrence of the eight phases of the Madden–Julian oscillation;
- (iii) SST+MJO, combinations of (i) and (ii); and
- (iv) weather types, the frequency of occurrence of the six circulation regimes identified in [Part I](#).

This set, when compared to the list proposed in [Part I](#), is missing only two candidate predictors (i.e., the SAM and SACZ indices); nonetheless, it still represents most of the observed variability.

A large number of statistical models were built using CCA for each one of the sets of candidate predictors indicated above, producing retrospective deterministic forecasts of frequency of extreme rainfall (dR95p) for the corresponding training period. CCA automatically computes orthogonal modes, the actual predictors, from the corresponding set of candidate predictors. The best models were selected by maximizing the spatially averaged Kendall's τ ; the skill scores were then computed for these models for the potential and real-time predictability experiments.

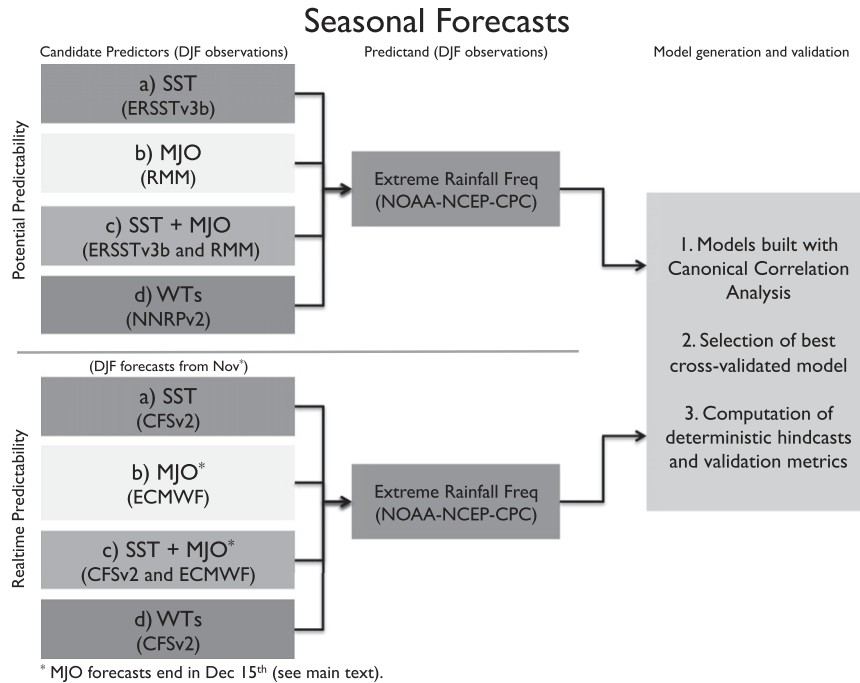


FIG. 1. Summary of the methodology followed to produce extreme rainfall seasonal forecasts.

2) SUBSEASONAL-TO-SEASONAL SCENARIOS

The general methodology used to produce s2s scenarios consists of two parts, and it is summarized in Fig. 2. The diagnostic part (steps 1–4 below) involves the identification of weather types and clusters of sequences of weather types conducive to particular s2s extreme

rainfall scenarios. The prognostic part (steps 5 and 6 below) builds and cross-validates the associated probabilistic forecast model. The steps are the following:

- 1) Compute the weather types from observations, and build the weather type daily sequences for each available season (i.e., the Klee diagram; see Part I for details).

Subseasonal-to-seasonal Scenarios

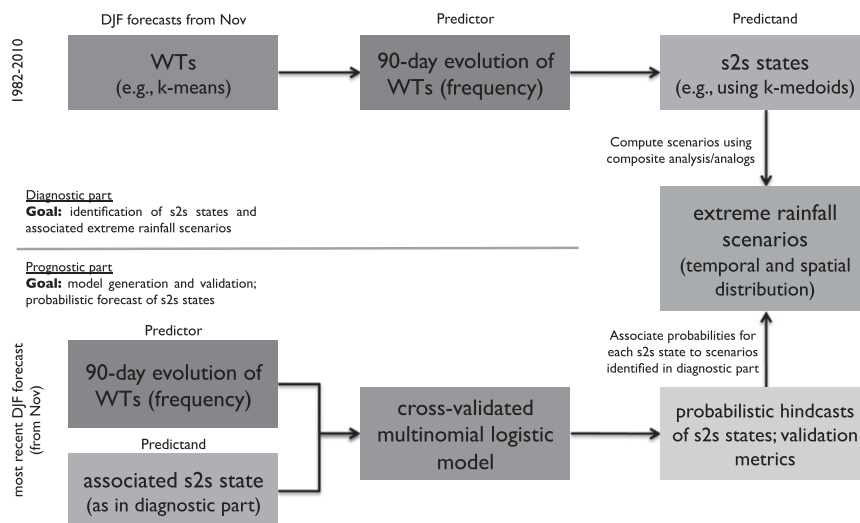


FIG. 2. Summary of the methodology followed to produce subseasonal-to-seasonal extreme rainfall scenarios.

- 2) Identify clusters of weather type sequences present in the Klee diagram (e.g., using the k -medoids algorithm). Each one of these new categorical clusters is a “typical representation” of the intraseasonal distribution of synoptic circulation regimes that are present in a particular season of the year (DJF, in this case). These categorical clusters are also referred to as s2s states.
- 3) Verify the physical consistency between the new categorical clusters and observed phenomenology (e.g., check that the obtained relationship between weather types’ occurrence, phases of candidate predictors, and extreme rainfall occurrence can be explained on a physical basis).
- 4) Compute the mean s2s rainfall scenarios. For each categorical cluster of weather types’ sequences, compute the associated spatial and temporal distribution of extreme rainfall via a composite analysis. This step provides information about when to expect extreme rainfall within a “typical season” of the categorical cluster under consideration and the spatial distribution of that rainfall.
- 5) Build the cross-validated probabilistic forecast model and analyze its predictive skill. Compute probabilities for each s2s state (i.e., for each predictand). There are different ways to do this. For statistical models this could be done, for example, via a multinomial logistic regression (see, e.g., [Moron et al. 2015](#)) using combinations of SST and MJO as predictors. For dynamical model output this could be done by first computing the model’s weather types and then linking corresponding categorical clusters to the observed ones. In this paper, a multinomial logistic model using frequencies of occurrence of weather types (forecast by CFSv2) is used to predict the observed s2s states.
- 6) Produce the s2s forecast scenarios for extreme rainfall events. Using the cross-validated forecast model, compute the probabilities for each one of the categorical clusters for the target season, and then use the corresponding s2s scenario identified in step 4. Note that it is then possible to associate the same probabilities to the occurrence of extreme rainfall events at subseasonal scale (e.g., weeks 3 and 4 or all of January), as they correspond to the complete sequence of weather types typified by the categorical clusters.

These steps present a basic methodology for producing s2s scenarios; more sophisticated ones will be explored elsewhere, as more complex models may be used (e.g., in steps 5 and 6) if necessary. In this approach the s2s states are being forecast and not the rainfall itself.

To illustrate the approach (see [Fig. 2](#)), only CFSv2’s weather type frequencies are used here as predictors (1982/83–2009/10) of s2s states, with a cross-validation window of 3 years, as the maximum likelihood estimator did not converge in several iterations of the cross-validation process when five years was tried. In step 5, the probabilities are rounded to the nearest integer, ensuring that the total probability is always 100%; to decide how to round the probabilities, the values leading to the best ignorance score ([Jolliffe and Stephenson 2012](#); [Mason et al. 2016](#)) are selected. More details about the methodology are discussed in [section 4](#).

The k -medoids algorithm ([Park and Jun 2009](#)) is used here to compute the s2s states. It is a partitioning method, similar to k means, commonly used in problems requiring robustness to outliers, arbitrary distance metrics, or when the mean or median does not have a clear definition. Most importantly, it works well with categorical data like the weather types. All the experiments reported here used the MATLAB implementation of the algorithm, with the Hamming distance function and 10 replications. The Hamming distance is an appropriate distance metric for categorical data, representing the percentage of the vector components that differ. After several experiments and comparison of how well the algorithm classifies the weather type sequences, the number of categorical clusters (i.e., medoids) was selected to be five. Although other values are statistically and physically plausible, increasing the number of clusters, and thus their actual similarity to the Klee diagram, reduces the sample available to compute the extreme rainfall s2s scenarios; on the other hand, using too few medoids tends to cluster states that have different characteristics.

The forecast models used in this approach are built using multinomial logistic regressions, fitting the coefficients that appear in [Eq. \(A2\)](#) via a maximum likelihood estimator and computing the probabilities for each scenario using [Eqs. \(A3\)](#) and [\(A4\)](#). This same type of model has been used recently by [Moron et al. \(2015\)](#) for similar purposes. For details see the [appendix](#).

The quantification of the predictive skill of this new s2s scenario methodology is not straightforward, as it involves the cross validation of both the weather types’ categorical clusters and the s2s extreme rainfall scenarios. For the purposes of this study, the hit score, hit skill score, and Kendall’s τ ([Jolliffe and Stephenson 2012](#); [Mason and Stephenson 2008](#)) are used as exploratory skill metrics for the models forecasting s2s states. In the present case the goal is not to forecast precise quantities (e.g., how many mm of rain) but to forecast the

most-likely distribution of days with extreme precipitation (scenarios).

3. Seasonal forecasts of extreme rainfall: Impact of cross-time scale interference on skill

This section explores the predictive skill of seasonal forecasts of weather statistics for SESA, in particular extreme rainfall frequency as measured by dR95p, comparing the use of predictors acting at multiple time scales against those acting at only one time scale. The next section discusses the subseasonal evolution of these weather statistics.

In a recent paper, [Moron et al. \(2015\)](#) studied the problem of retrospectively forecasting the frequency of weather types for the Maritime Continent, given perfect knowledge of three regional climate drivers—namely, the annual cycle, the Niño-3.4 index, and MJO phases. They found that indeed the predictive skill was higher when they considered a model with all these predictors simultaneously. Although their results add evidence to support the cross-time scale interference idea, more research is required, for example, to analyze these interferences in global circulation models.

A common assumption is that dynamical models consider these cross-time scale interactions in a “natural” way. However, several global circulation models are not representing well key observed interferences, and dynamical downscaling does not necessarily improve the situation ([Muñoz and Goddard 2014](#)).

In this section, the predictive skill is analyzed both for the observed behavior of the selected candidate predictors (potential skill) and for the case of actual forecasts (real-time skill). For the latter the output of two dynamical models, CFSv2 and the ECMWF, are used as predictors; for details see [section 2](#).

Although the length of skillful MJO predictions for CFSv2 is still considerably shorter than that for ECMWF, CFSv2 does a remarkable job capturing observed cross-time scale interactions. The general spatial structures associated with the observed weather types are reproduced by CFSv2 ([Fig. 3](#)), at least for the DJF season, with no need to project the model’s fields into the observed EOF patterns. Regarding the representation of the weather types’ temporal evolution, the skill scores indicate also a good representation of the observed behavior, in spite of the fact that the total proportion of occurrence of each circulation regime still requires some improvement (cf. number of days in parentheses for both observed and modeled weather types in [Fig. 3](#)). Further research is required to explore how well this and other dynamical models reproduce weather type characteristics and their relation to cross-time scale

interferences. As discussed in [Part I](#), this analysis can indicate concrete improvements to be performed on the global and regional climate models based on physical interactions.

The skill metrics chosen are a measure of how good the forecasts are, but they characterize different attributes, and since their values are different in different locations, they are presented in terms of spatial maps ([Figs. 4 and 5](#)). The Spearman correlation coefficient shows how in phase the observations and forecasts are. Discrimination, or how well a forecast distinguishes between the different categories, indicates whether any potentially useful information is actually being provided. ROC area maps (the areas under ROC curves compare proportion of hit rates versus false alarms) are used here to show the spatial distribution of the model’s discrimination. Furthermore, the Kendall’s τ coefficient is used as an overall goodness index of the prediction, a measure of each model’s mean extreme rainfall predictability over SESA. The analysis of skill is presented in the following paragraphs at local ([Figs. 4 and 5](#)) and regional scales ([Table 1](#)).

In general, when a particular model is considered, the spatial patterns exhibited in the different skill metrics are very similar ([Figs. 4 and 5](#)), indicating that there are certain locations in SESA where forecasts are both in phase with observations and show good discrimination for the above-normal and below-normal categories. When the different models are considered, it is noticeable that these regions tend to be confined to Argentina, northern Uruguay, and Brazil in the SST or MJO models, but cross-time scale models (i.e., SST+MJO and weather types) exhibit wider areas with even higher skill than the others, including almost all of Uruguay and southern Brazil. Overall, the lowest skill is found along the northern and western boundaries of SESA.

Although the skill scores between the potential and real-time predictability experiments cannot be directly compared because of different training periods (28 and 16 yr, respectively), it is noticeable that the skill metrics for actual forecasts exhibit higher variability (statistical range of the values): the forecasts tend to be very good in certain regions and considerably bad in others. In the potential predictability experiments, the skill is more spatially homogeneous: forecasts tend to be very good in most places and not particularly good in a few. Models considering cross-time scale interferences (SST+MJO and weather types; [Figs. 4 and 5](#), bottom two rows) show the best skill scores for both potential and real-time predictability experiments, in agreement with the cross-time scale interference hypothesis. Although these two models show statistically significant Spearman

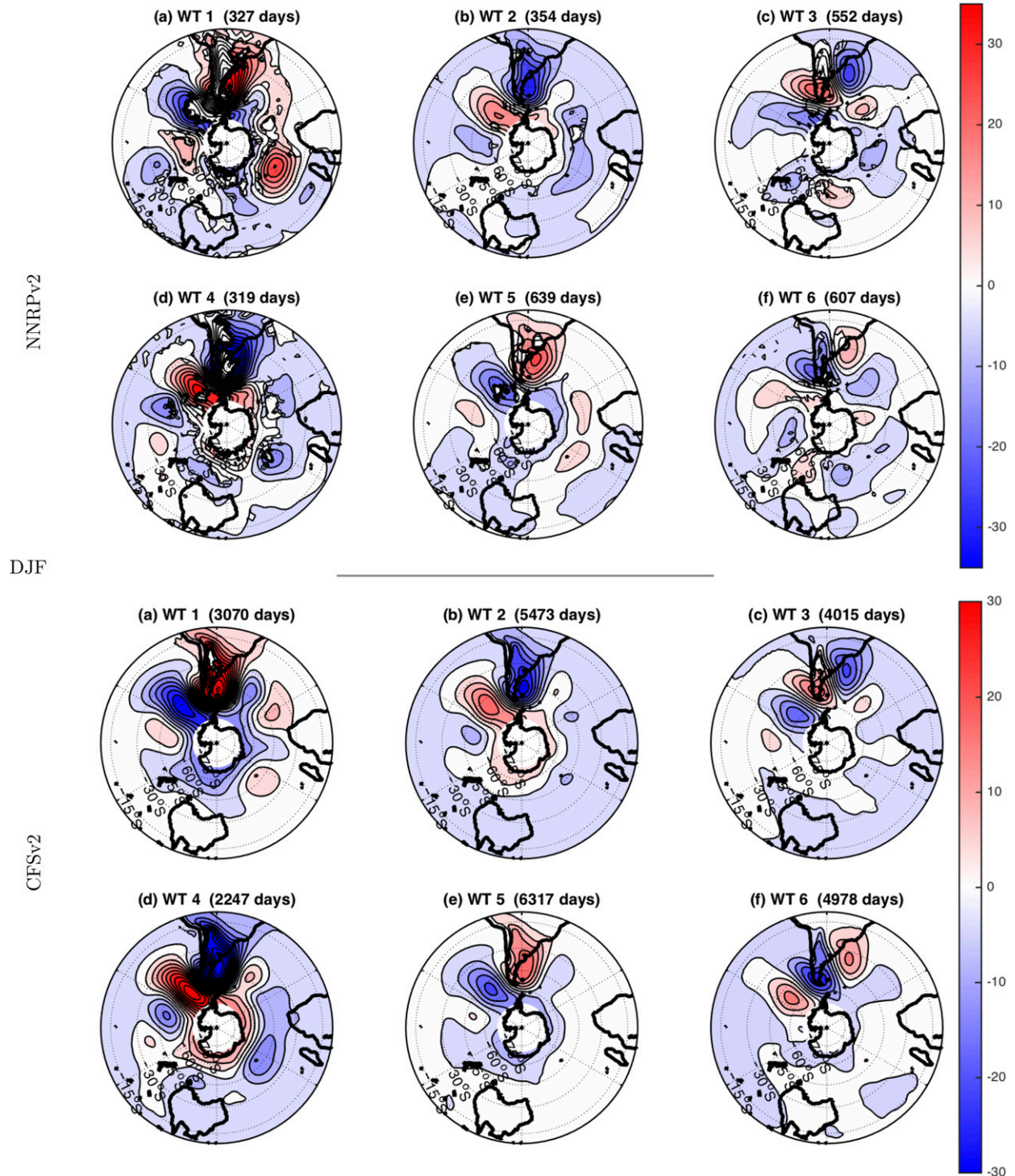


FIG. 3. (top) Observed (designated as NNRpv2) and (bottom) modeled (designated as CFSv2) weather types for the DJF season. Contours sketch geopotential height anomalies (gpm; contour interval is 5 gpm), and shaded regions indicate statistically significant ($p \leq 0.05$, Student's t test) anomalies. Panel titles give the accumulated number of days for all the DJF seasons assigned to each weather type (WT). Note that the CFSv2 weather types were computed after concatenating 10 members, and thus the total number of days is 10 times that of one member.

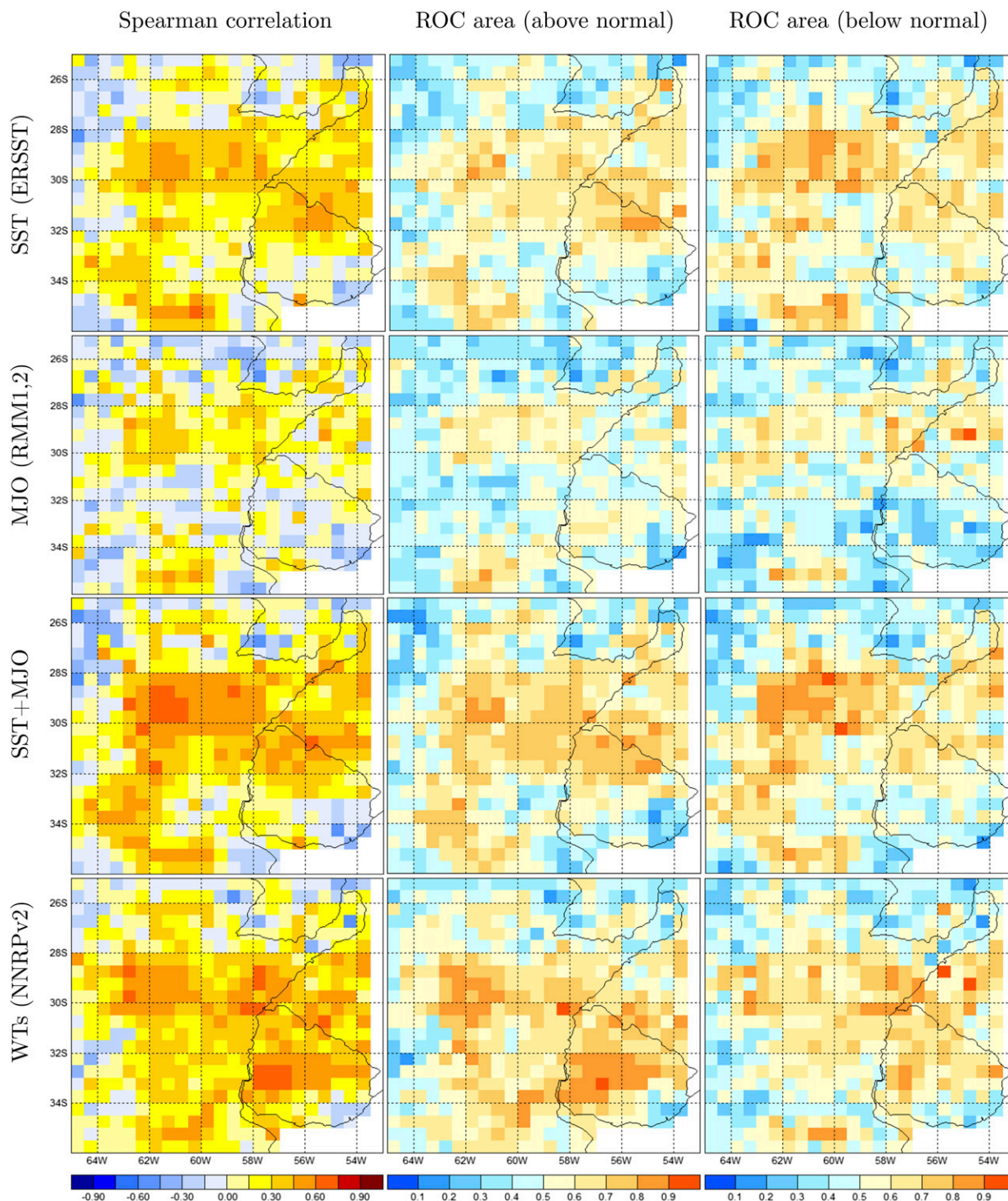


FIG. 4. Comparison of different hindcast attributes for the potential predictability experiments (observed predictors) shown in Table 1.

correlation coefficients (>0.30 for $p < 0.05$) for a very large number of grid boxes, the weather type model exhibits better skill for basically all of Uruguay as well as southern Brazil and regions of Argentina.

The ROC areas tend to be better for the above-normal category in the cross-time scale models, except for the potential predictability SST+MJO model (Fig. 4), which exhibits better discrimination for the

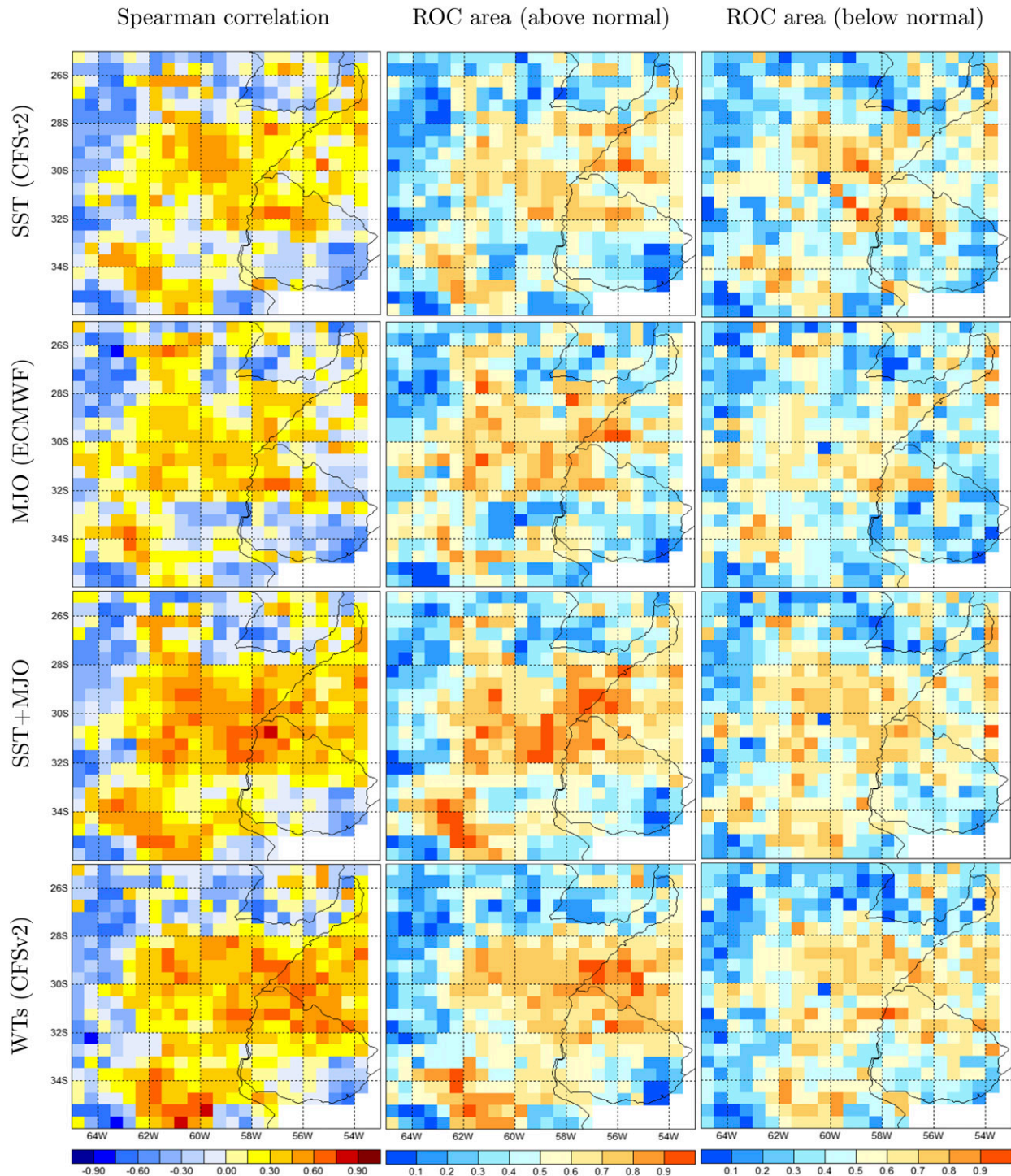


FIG. 5. Comparison of different hindcast attributes for the real-time predictability experiments (forecast predictors) shown in Table 1.

below-normal category in a region of Argentina close to the center of SESA. Although the differences between the cross-time scale models seem to be mainly in the location and spatial extension of the regions with higher skill scores (Figs. 4 and 5), regionwide averages of the

metrics show slightly higher values for the weather type model, as discussed in the next paragraph.

The differences between the models could also be studied at regional scale. Spatially averaged Kendall's τ for the MJO model (potential and real-time hindcasts)

TABLE 1. Spatially averaged potential (observed predictors, 28 yr) and real-time (forecast predictors, 16 yr) skill for the different models selected. For each column, SST models are used as reference to compute statistically significant differences ($p \leq 0.1$, denoted by an asterisk).

Predictor and model	Kendall's τ (potential)	Kendall's τ (real time)
SST	0.174	0.163
MJO	0.118*	0.134*
SST+MJO	0.231*	0.192*
Weather types (WTs)	0.249*	0.202*

is significantly different but lower than the SST model (see top rows of Table 1). For the real-time case, the MJO and SST models' difference in Kendall's τ is lower than for the potential predictability experiment.

This relative increase of skill is attributed here to the fact that the MJO ensemble forecast product provided by ECMWF actually includes 121 past observed days (14 July–12 November) in addition to the 32 forecast days (13 November–15 December). The analysis of the different experiments (using only the 121 past observed days, only the 32 forecast days, and both) suggests that, because of the quasi-regularity of the MJO, skillful DJF forecasts can be achieved using past phases of the MJO as predictors. The best skill was found when both observed and forecast phases are mixed and used as (lagged) predictors for DJF. This is not surprising, as the relatively long period used is providing 1) a better specification of the MJO states (phases) for each particular year considered and 2) a decrease of the sampling error, as a total of 153 days is used instead of only 32.

The Kendall's τ for the SST+MJO model exhibits higher and significantly different values than the SST model (Table 1), in agreement with the hypothesis. Note that the SST+MJO model uses a combination of CFSv2 DJF's SSTs, initialized in October, and ECMWF's MJO phases from the 13 November forecast cycle. The skill of the SST+MJO model is high, even when the MJO forecast is only for 32 days from mid-November, and thus it does not cover the entire DJF season. This result suggests that the observed frequency of MJO phases in the months previous to the target season could be used as a potential predictor for extreme rainfall in SESA, and it merits further study.

Although at local scale the SST+MJO model tends to outperform all the others (Figs. 4 and 5, third row from top), the spatially averaged Kendall's τ of the model using weather types is the highest (Table 1). The fact that this model's regional skill is not significantly ($p < 0.05$) different than the one associated with the SST+MJO model is consistent with what was suggested

in Part I about the weather types being “especially sensitive” to cross-time scale interactions. It is likely that these circulation regimes are not only capturing these interferences at subseasonal-to-seasonal scales but also sensitive to interferences of climate drivers at other time scales. Another way to explain that their predictability is higher than the monoscale models (SST and MJO) is related to the fact that the weather types are proxies of the physically available states of the subsystem associated with distinctive atmospheric circulations in SESA. Hence, any extreme rainfall event could be written only in terms of these weather types because they are a filtered version of the physical field that increases the predictive skill. If the weather types are a set of vector bases to describe the vector space of all possible observations, and it is true that multiple time-scale climate drivers interfere with each other in order to produce these observations, then it is logical that the weather types are sensitive to cross-time scale interactions.

Notwithstanding that DJF's mean and extreme rainfall are more difficult to forecast than other seasons (Almeira and Scian 2006; Pisciotto et al. 1994; Cazes-Boezio et al. 2003), there is a significant increase in potential and real-time predictability (Table 1) when cross-time scale interactions are considered by statistical models. A CCA-based MOS applied on a combination of CFSv2 and ECMWF outputs could be used as an element of an experimental forecast system for frequency of extreme events in SESA for DJF and probably for other seasons (and locations), too. For models using weather types as predictors, the skill is expected to be even higher than the one reported here when other methods are used instead of the CCA approach, as in Moron et al. (2010). This idea will be analyzed elsewhere.

The next section takes advantage of the high skill found in the weather type model to build s2s extreme rainfall scenarios from 3-month daily sequences of CFSv2's circulation regimes.

4. Subseasonal-to-seasonal extreme rainfall scenarios

The previous section provided evidence that the predictive skill for the occurrence of extreme rainfall events in SESA increases when the interactions of predictors at different time scales are considered. This section discusses a predictive approach for the subseasonal evolution of these extreme events.

It is possible that the increase of skill is achieved just by involving additional independent predictors, with no interference taking place between them. In that case, even if the predictors do not interact with each other, the

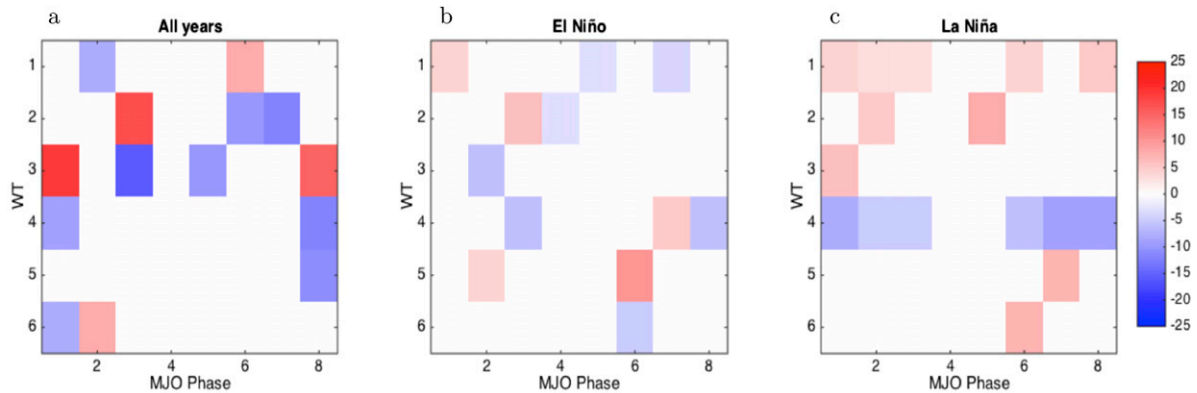


FIG. 6. Anomalous percentage of occurrence (see color bar) of each weather type for each phase of the MJO for (a) all seasons (DJF 1982–2010), (b) El Niño events, and (c) La Niña events. Colored tiles are significant at the $p \leq 0.05$ confidence level, obtained using a bootstrapping method resampling 1000 times.

rainfall field in the region could still be explained by their complementary signals.

A second possible explanation is that, in addition to the case above, there is an increase in the predictive skill because the nonlinear interference of climate drivers is itself an additional predictor. This would introduce selection rules that could increase predictive capacity: the interaction is reducing the vector space of all possible forecasts for a particular target period, from the wide range of outcomes associated with an El Niño event to, for example, the ones that involve simultaneously an El Niño event and MJO locked in phase 3.

To explore these ideas, statistically significant ($p \leq 0.05$) anomalous percentage of the observed occurrences of weather types were computed for each MJO phase considering all years, the five strongest El Niños on record, and the five strongest La Niñas on record (Figs. 6a, 6b, and 6c, respectively). Preferred occurrences of the weather types in relation to the eight phases of the MJO were found in each case, indicating that in general the associated conditional probabilities are not equal (using Dirac's notation to be consistent with Part I and ENSO^+ denoting El Niño, ENSO^- denoting La Niña, and WT the set of weather types):

$$|\langle \text{WT} | \text{MJO} \rangle|^2 \neq |\langle \text{WT} | \text{MJO}, \text{ENSO}^{(+,-)} \rangle|^2 \quad \text{and} \quad (1)$$

$$|\langle \text{WT} | \text{MJO}, \text{ENSO}^+ \rangle|^2 \neq |\langle \text{WT} | \text{MJO}, \text{ENSO}^- \rangle|^2. \quad (2)$$

Also, since Part I showed that the weather types do not tend to persist for many days (see Table 1 of Part I), Eqs. (1) and (2) suggest that particular weather types' sequences may be more common in the presence of specific interactions.

These results suggest that cross-time scale interferences produce distinctive preconditioning or entanglements between the climate drivers whose impacts (e.g., on

extreme rainfall) could be represented in terms of typical s2s scenarios built using sequences of daily circulation regimes (weather types). Since the previous section showed that those seasonal forecasts for DJF are skillful, in what follows seasonal sequences (i.e., sequences over the 3-month season) will be used to define s2s states (in principle, weekly or monthly sequences could be used too, but no skill analysis has been performed here for those time scales).

Note that these ideas are in line with the approach to extract subseasonal scenarios considered by Moron et al. (2013), although the methodology followed here is different: while their subseasonal scenarios are built in terms of the rainfall field itself, the present study uses seasonal sequences of weather types, which are more predictable than rainfall, to identify states that are then related to subseasonal-to-seasonal scenarios of occurrence of extreme precipitation. One may think of this approach as a type of analog method (Lorenz 1969; Zorita and von Storch 1999; Van den Dool 1994) that uses the s2s states to identify the analog years but that provides the subseasonal-to-seasonal evolution of the extreme events. Further details about the present approach are discussed in the following subsections.

a. Subseasonal-to-seasonal states and extreme rainfall scenarios

In this subsection we illustrate the general methodology, summarized in section 2, for the particular case in which the predictor is a set of seasonal frequencies of weather types, computed from daily sequences produced by CFSv2 (see Fig. 2). These are the same combinations of weather types used in the predictability experiments reported in section 3, already known to provide statistically significant cross-validated skill.

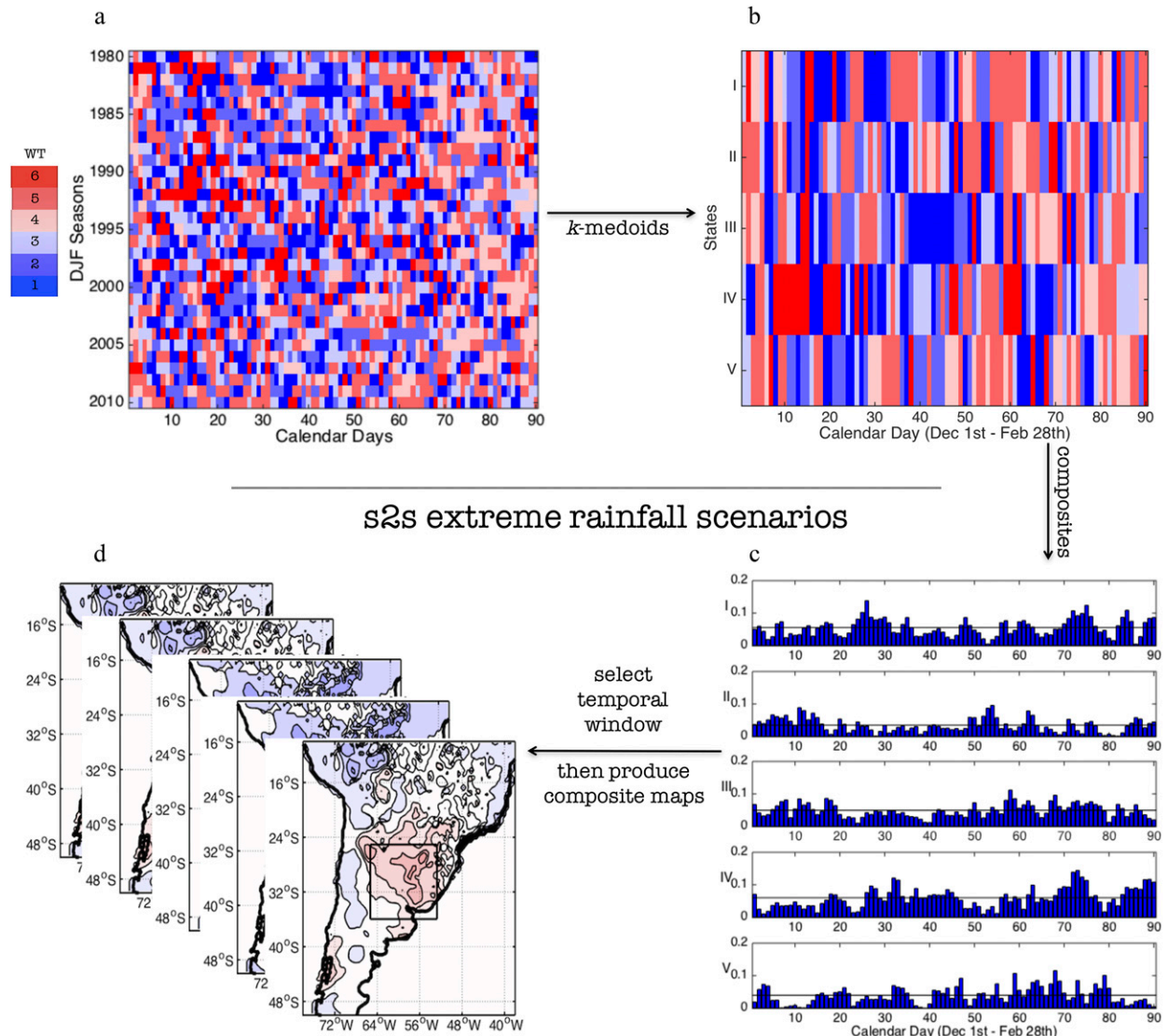


FIG. 7. Illustration of the methodology followed to generate s2s extreme rainfall scenarios. (a) Klee diagram showing all observed weather types—blue tends to be related to negative rainfall anomalies, and red tends to be positive rainfall anomalies; (b) subseasonal-to-seasonal categorical clusters (or states) showing 90-day sequences of weather types; (c) temporal evolution of each observed s2s extreme rainfall scenario (mean frequency of extreme rainfall events per day per grid box—these values correspond to dividing the fifth column of Table 2 by the number of days in the season with extreme events); and (d) spatial distributions of the s2s extreme rainfall scenarios.

The weather types and associated Klee diagram, showing the sequences of circulation regimes for every day in all the DJF seasons under analysis, were computed following the same methodology reported in Part I (Fig. 7a).

Then the s2s states were obtained via a categorical clustering algorithm (Fig. 7b) of the daily sequences of weather types along the entire season, for all years in the period. In the present study, after several tests, a set of five clusters was considered adequate to represent different entangled states conducive to specific distributions of occurrences of extreme rainfall (dR95p

index). As mentioned before, the hypothesis is that these s2s states represent distinctive cross-time scale interactions and thus are not modulated by just one climate driver. Although there are s2s states that are clearly preferred during different ENSO phases (e.g., El Niño events in state I and La Niña events in state V), ENSO years tend to appear in other clusters too (Table 2).

The next step involves the identification of the s2s rainfall scenarios via a composite analysis of the dR95p fields associated with each s2s state. The highest frequency of extreme precipitation events, or extremely

TABLE 2. Years of occurrence for each subseasonal-to-seasonal state, number of years belonging to that state, approximate periods of occurrence (in calendar days for the DJF season) of extremely wet days, and mean seasonal occurrence per grid box. Years denote the end of the season (e.g., 1998 corresponds to 1997/98).

S2s state	Years	Sample	Extremely wet spells (calendar days)	Extreme occurrence
I	1982, 1986, 1996, 1998, 2003, 2007, 2009, 2010	8	20–30, 55–65, 70–80, and 80–90	Frequent (28.0 days)
II	1989, 1991, 1995, 1997, 2006, 2008	6	5–15, 49–65, and >85	Very infrequent (17.5 days)
III	1980, 1983, 1985, 1988, 1990, 1993, 1994, 2005	8	5–20 and 55–80	Moderate (25.0 days)
IV	1981, 1984, 1987, 1992, 2004	5	25–45, 65–75, and >83	Very frequent (30.4 days)
V	1999, 2000, 2001, 2002	4	60–80	Infrequent (19.9 days)

“wet spells,”² tends to occur during specific calendar days (Table 2 and Fig. 7c). Though these spells are often associated with sequences of weather types involving weather type 4 and weather type 6 (Part I), this clearly is not always the case; persistence, ordering, and alternation of the different circulation regimes are important to understand the presence or not of extreme precipitation events—similar to how a particular set of letters in a word mean something different when they are rearranged. For details, see Part I.

The s2s rainfall scenarios are not only different with respect to the way spells are distributed along the season, but also in their seasonal average number of days with extreme rainfall: scenarios IV and II have the highest (~30 days) and lowest (~17 days) frequencies of events, respectively; scenarios I, III, and V are intermediate ones (~28, 25, and 20 days, respectively).

Additional information for each scenario could be obtained in terms of the spatial distribution of (extreme) rainfall for a particular temporal window (Fig. 7d; e.g., days 20–30), the middle month, or the entire season. This approach allows for the identification of possible locations where preparatory actions may be implemented before the occurrence of the extreme events.

The same methodology could be used for different percentiles of precipitation (and other variables), although an evaluation of its performance for these other cases must still be explored.

b. Forecast skill

In this approach the s2s states (the categorical clusters) are the ones being forecast and not directly the temporal or spatial distribution of extreme rainfall. The validation metrics considered in this section are computed to evaluate discrimination, reliability, and resolution (Jolliffe and Stephenson 2012; Mason and Stephenson 2008) of the categorical forecasts of sequences of weather types. The joint validation of both the s2s states and scenarios will be considered elsewhere.

Despite the fact that the best-guess multinomial logistic model exhibits hits for only half of the forecasts (Table 3), it is still a relatively high frequency of hits when compared to the climatological one (0.2 if equiprobability is assumed true for this case and 0.14–0.28 if more precise values are computed from the samples indicated in Table 2). Further analysis reveals statistically significant ($p < 0.05$; bootstrapping method resampling 1000 times) values of the scores under consideration: hit score (0.5), hit skill score (0.375), and

TABLE 3. Cross-validated forecast probabilities (%) for DJF for each s2s state and the observed state. Results are shown for the best-guess multinomial logistic model. Probabilities have been rounded to the nearest integer leading to the best expected ignorance score (see section 2 for details).

Year	I	II	III	IV	V	Observed	Hit (H) or miss (M)
1982/83	1	53	41	4	1	III	M
1983/84	1	8	60	30	1	IV	M
1984/85	1	31	57	11	1	III	H
1985/86	96	1	1	1	1	I	H
1986/87	1	33	43	21	1	IV	M
1987/88	1	9	24	65	1	III	M
1988/89	1	50	44	4	1	II	H
1989/90	1	29	49	20	1	III	H
1990/91	1	2	1	1	95	II	M
1991/92	1	9	25	64	1	IV	H
1992/93	82	1	15	1	1	III	M
1993/94	1	15	66	17	1	III	H
1994/95	1	44	17	36	1	II	H
1995/96	58	18	21	2	1	I	H
1996/97	1	18	36	44	1	II	M
1997/98	96	1	1	1	1	I	H
1998/99	1	1	1	1	96	V	H
1999/00	18	1	10	38	33	V	M
2000/01	96	1	1	1	1	V	M
2001/02	1	67	1	2	28	V	M
2002/03	96	1	1	1	1	I	H
2003/04	1	31	13	54	1	IV	H
2004/05	66	11	19	3	1	III	M
2005/06	1	4	7	1	87	II	M
2006/07	96	1	1	1	1	I	H
2007/08	1	94	1	2	1	II	H
2008/09	25	18	37	3	17	I	M
2009/10	1	56	38	5	1	I	M

² Although these do not correspond to a formal definition of wet spells, the name has been adopted here for the sake of simplicity.

TABLE 4. Contingency table (% of the total no. of years) for the hindcasts reported in Table 3.

Forecast	Observed				
	I	II	III	IV	V
I	18.0	0.0	7.1	0.0	3.6
II	3.6	10.7	3.6	0.0	3.6
III	3.6	0.0	10.7	7.1	0.0
IV	0.0	3.6	3.6	7.1	3.6
V	0.0	7.1	0.0	0.0	3.6

Kendall's τ (0.338). The last one is considerably higher than the corresponding potential skill value obtained in section 3 for the seasonal frequency of extremely wet days (see Table 1; note that the present results use the same number of years as the potential skill experiments).

Additional characteristics of the predictive model are summarized with a contingency table (or confusion matrix; Table 4). The model's forecasts are better for state I (18% of all years), followed by states II and III (both with 10.7%). The worst forecast occurs for state V (3.6%), with a tendency to be confused only by state II. Note that the latter is similar to state V, having the second minimum average frequency of days with extreme rainfall in the entire season. State IV (7.1%) tends to be equally confused with states II, III, and V, but not with state I (see Table 4).

The present version of the method does not provide specific forecasts of the expected extreme rainfall distribution, but rather a composite analysis involving similar years in the historical record. That is why the outputs have been called "scenarios" here. Nonetheless, it is argued that the information provided is useful for decision-makers, as each s2s extreme rainfall scenario involves only a handful of real historical cases that stakeholders directly know or have indirect experience with. For instance, to suggest that DJF 2015/16 could be classified as state I, with an extreme rainfall scenario similar to the one presented at the top of Fig. 7c, provides information about the typical distribution of extremes (e.g., mainly at the end of December and during the second half of February), and also indicates that it belongs to a particular set of years that, in the most part, were moderate and strong El Niño events. Decision-makers can then refer to past experience to understand and estimate possible impacts.

Finally, note that the best forecast category, state I, is one of the most impactful, as it is associated with high seasonal frequency of extreme rainfall events. It is also one of the most common categories, and thus society may be more used to dealing with the associated hazard under its present vulnerabilities. Those two facts give

additional value to the use of this methodology to produce subseasonal-to-seasonal scenarios.

c. Two contrasting examples: 2006/07 versus 2000/01

This subsection discusses the s2s states and extreme rainfall scenarios obtained for two particular DJF seasons, 2006/07 and 2000/01. The forecast model assigned the same probability distribution for each s2s state in those years (Table 3), but it was only correct in one of those cases: 2006/07.

Analysis of the observed daily evolution of the circulation regimes (Fig. 8a) indicates that the 90-day sequence for 2006/07 was correctly identified by the multinomial logistic model using the corresponding seasonal frequency of weather types.

On the other hand, the k -medoids algorithm identified the observed sequences for 2000/01 as a realization of state V (Fig. 8a). The wrong 2000/01 forecast is attributed to a close similarity between the weather type's seasonal frequencies for that period, and the corresponding values for state I. This is the only case in the study in which the CFSv2's frequency distribution of the circulation regimes failed as a classifier for state I (Table 3).

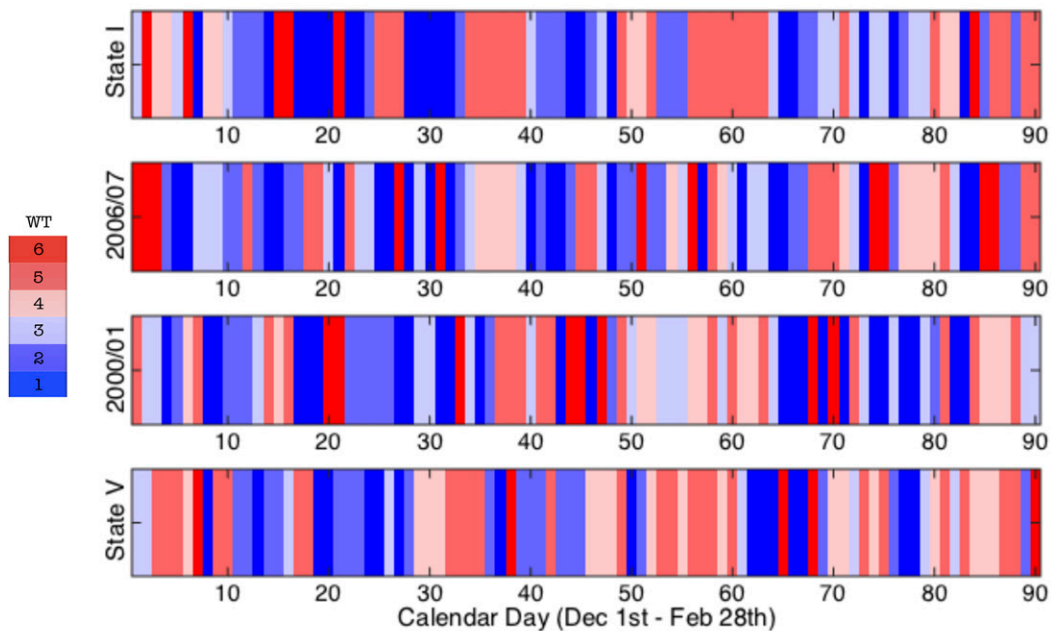
The extreme rainfall evolution for 2006/07 exhibits a statistically significant Spearman correlation ($p < 0.01$; see Fig. 8b) with scenario I. In contrast, the evolution of extremes for 2000/01 is only significantly correlated ($p < 0.01$) with scenario V, as one should expect.

The spatial distribution of the frequency of rainfall extremes is consistent with the temporal evolution analysis. Statistically significant pattern correlations ($p < 0.01$) are only achieved between scenario I (Fig. 9a) and the 2006/07 season (Fig. 9b) and for scenario V and the 2000/01 season (Figs. 9c,d).

The 2006/07 season involved the occurrence of extreme rainfall events distributed more or less homogeneously over all SESA, as in scenario I, while 2000/01 presented a spatial pattern with more extremes along the western and northern boundaries of SESA; note that although scenario V shows the same distribution, it has a noticeable accumulation of extremes along the southwestern boundary of SESA that does not appear in the 2000/01 map.

The failure in the 2000/01 forecast is mostly related to a misidentification of the correct scenario (V, and not I). This situation, at least for the cases considered, is expected to improve if the actual forecast sequence of weather types is used instead of the forecast seasonal frequency of the regimes. Although this idea involves some methodological experimentation to identify the best way to use multimember sequences of weather types, it is considered feasible and it will be treated in a future work.

a. WT sequences



b. dR95p

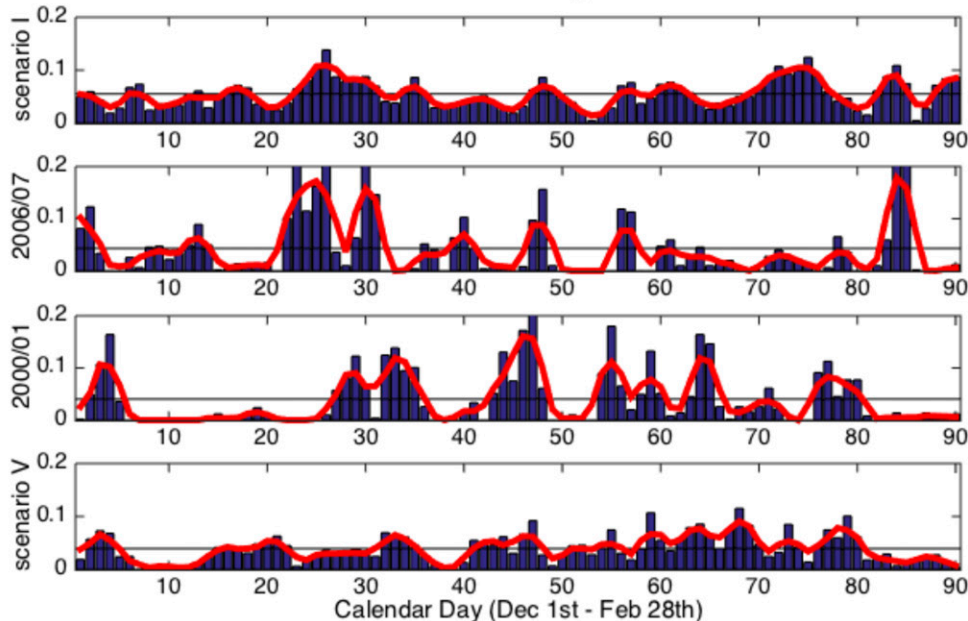


FIG. 8. Temporal evolution of (a) daily WT sequences and (b) frequency of rainfall extreme events (dark blue bars; red curves show 3-day moving averages). States I–V and scenarios I–V were produced by the methodology discussed in section 2. DJF 2006/07 and 2000/01 correspond to observations.

5. Real-time forecast constraints

This section briefly describes some operational aspects of an experimental forecast system for s2s extreme rainfall scenarios in SESA.

It is recommended to use the best predictors found in the present study (i.e., SST+MJO and weather types). As indicated, the required forecasts involve both the ECMWF (MJO) and CFSv2 (SST and weather types) models.

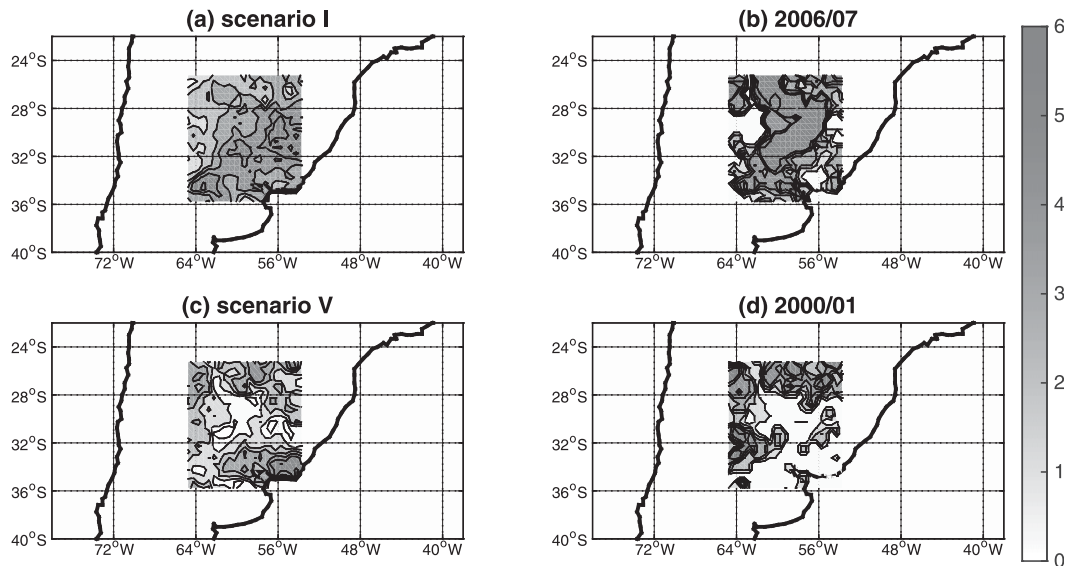


FIG. 9. Spatial distribution of the frequency of extreme rainfall events for (a) scenario I, (b) DJF 2006/07, (c) scenario V, and (d) DJF 2000/01. Units are frequency of extreme events per season per grid box. The contour interval is unitary.

The analysis performed in the present study involved data made available each year around 15 November for CFSv2 [initialized in October; see details in [Saha and Tripp \(2011\)](#)] and around 13 November for ECMWF. This means that the operational forecasts could start on 15 November and thus use all the required fields. An alternative is to use October's observed SST fields made available around 5 November (or even CFSv2 output made available in October, initialized in September) and the ECMWF MJO forecasts made available on 6 November, which means that the start date for the operational forecast in this case could be 6 November (note that the skill for this alternative has not been analyzed in this paper).

As explained in [section 2](#), the required CFSv2's forecasts are SST anomalies (DJF, monthly resolution) and geopotential height anomalies at 850 hPa (DJF, daily resolution), from which the frequency of occurrence of the set of six weather types can be easily obtained (see [Part I](#) and [section 2](#) for details). In the case of the ECMWF, the ensemble forecast for the two PCs is used to compute the frequency of occurrence of MJO phases. Their five-member ensemble contains a total of 153 days (121 past observations plus 32 actual days of forecast), which are to be used without subtracting any subset.

With these datasets, it is possible to produce both seasonal forecasts of occurrence of extreme rainfall and s2s extreme rainfall scenarios, following the methodology discussed in the previous pages. Automating the process will decrease the probability of mistakes and guarantee that the products will be issued on time; while

the details are out of the scope of the present paper, it will only be mentioned here that both types of products could be run automatically using scripts for the Linux version of CPT and MATLAB, providing also updated cross-validated skill metrics.

6. Conclusions

The forecast skill of extreme rainfall frequency in southeastern South America is improved for the DJF season when the interference of predictors at different time scales is considered. This is attributed to mechanisms of climate variability acting at one time scale that contribute to predictability at other time scales.

Seasonal forecasts for frequency of daily rainfall exceeding the 95th percentile are, at regional scale, significantly more skillful when cross-time scale predictors are used, compared to models employing SST fields alone (e.g., Kendall's τ increases $\sim 23\%$ – 43%). This improvement allows for the provision of skillful forecasts to decision-makers in the region as a whole, in terms of seasonal probabilities of occurrence of extreme rainfall events for the three traditional categories: above normal, below normal, and normal. However, at the local scale of a particular grid box, the use of cross-time scale predictors may not always increase the skill, possibly as a result of local noise patterns that are filtered out when a regional average is performed.

Since additional climate information at shorter time scales, such as the likely evolution of the extreme events within the season, is widely desired by decision-makers,

a seamless subseasonal-to-seasonal forecast methodology was developed and tested. The new predictive approach is based on cross-time scale interferences in order to provide a better specification of the state of the predictor(s) in the models and thus achieve more skillful forecasts.

These interactions provide seasonal predictability of weather statistics (extreme rainfall frequency in this case) that can be exploited to produce subseasonal-scale climate information about the evolution of such weather statistics. The approach described in this paper allows for the probabilities to be computed for each one of five (in the case analyzed here) states that describe seasonal sequences of daily circulation regimes conducive to particular extreme rainfall distributions. These scenarios are associated with distinctive periods of time and frequencies of occurrence of extremely wet spells (e.g., during the first 20 days of the season or along the entire month of February, like in scenario III). Although these are not forecasts of the weather evolution per se (i.e., the subseasonal-to-seasonal states are the ones being forecast), the approach offers useful information to decision-makers interested not only in how many extreme events will happen in the season but also in how, when, and where those events will occur.

Besides exploiting seasonal predictability to provide information at subseasonal scale, the subseasonal-to-seasonal states have the advantage of being more predictable than rainfall scenarios, because the atmospheric circulation patterns are in general more predictable than rainfall regimes. Moreover, preliminary results show that this approach provides consistent results when applied to other parts of the world, and it also seems to increase the skill of mean seasonal values (i.e., not only extremes).

The particular processes by which cross-time scale interferences increase forecast skill in different parts of the world are not well understood. Although the role of weather types and their relationship to different physical mechanisms was discussed in Part I to explain the occurrence of extreme rainfall events in SESA, further research is required in order to better understand how the cross-time scale interactions produce the subseasonal-to-seasonal states associated with specific intraseasonal evolution of extremes. The physical mechanisms behind sequences of weather types (or words, to use the analogy of Part I) are more complex than just adding up the processes associated with daily events (i.e., the memory of the system is important), underscoring the nonlinear nature of the interferences.

Indeed, from a system dynamics perspective (Palmer 1999), extreme rainfall in SESA and its predictability may be ruled by the effect of a linear or nonlinear superposition of noninteracting or interacting climate drivers. Which one is the case for SESA? The present

research indicates that the best predictor is a nonlinear function of the original climate drivers considered. Moreover, the best forecasts for extreme rainfall frequency (at least for SESA and DJF) are obtained via a nonlinear function of the candidate predictors. Studies in other parts of the world have found similar results when studying interactions between climate drivers (see, e.g., Yoo et al. 2010; Krishnamurthy and Shukla 2008; and references therein).

From this perspective, the nonlinearity of the interferences, the seasonal weather statistics, and the subseasonal evolution are all related. Once the entangled state is established, in addition to modulating the seasonal frequency of extreme events, the cross-time scale interactions lead to intraseasonal evolution of extreme rainfall that happens in a more organized, or less random, way throughout the season. For example, the subseasonal-to-seasonal state I (Fig. 7), which tends to occur during El Niño events and thus with the presence of frequent meridionally propagating Rossby waves affecting SESA (Part I), is associated not only with the highest seasonal frequency of extreme rainfall events, but this state tends to happen during the end of December and the middle of February.

As a final comment, a simple version of the subseasonal-to-seasonal scenario approach was discussed in this paper. It is recommended the extensions of this method be explored, for example, using Markov chains instead of a composite analysis.

Acknowledgments. The authors are grateful to two anonymous reviewers, Vincent Moron, Cathy Vaughan, Walter Baethgen, and Yochanan Kushnir for stimulating discussions about different aspects of the paper; to Frederic Vitart (ECMWF) for providing the MJO forecasts used in this research; and to Mike Bell and Rémi Cousin, from the IRI Data Library Team, for their invaluable help making available several datasets and some obscure Ingrid coding routines. This work was supported by the National Science Foundation project AGS1049066 (SESA project), and it was part of Muñoz's doctoral thesis as Faculty Fellow at the Department of Earth and Environmental Sciences (DEES) of Columbia University. Robertson was supported by ONR MURI Grant N00014-12-1-0911. The authors declare no conflict of interests.

APPENDIX

Multinomial Logistic Models

This study employs multinomial logistic models, as mentioned in step 5 of section 2b(2), to forecast the s2s states using the chosen set of predictors.

If π_i denotes the conditional probability associated with the i th s2s state (categorical cluster Y_i , $\forall i = 1, \dots, n$), given a predictive state vector \mathbf{X} —that is, a combination of p predictors (X_j , $\forall j = 1, \dots, p$)—then, using Dirac's notation to be consistent with Part I,

$$\pi_i = |\langle Y_i | \mathbf{X} \rangle|^2 = P(Y_i | \mathbf{X}), \quad (\text{A1})$$

and the multinomial logistic model can be written as

$$\log \frac{\pi_i}{\tilde{\pi}} = \alpha_i + \beta_{ij} X_j, \quad (\text{A2})$$

where the Einstein summation convention is used, $\tilde{\pi}$ denotes the probability of the $n - 1$ reference category logits, α_i is a constant associated with the i th s2s state, and β_{ij} is the coefficient of each predictor X_j , representing the effects of the predictor variables on the relative risk or log odds of being in one category versus the reference category.

From Eq. (A2) it is possible to write $\forall i = 1, \dots, n - 1$ as follows:

$$\pi_i = \frac{\exp(\alpha_i + \beta_{ij} X_j)}{1 + [\exp(\alpha_k + \beta_{kj} X_j)]_k} \quad \text{and} \quad (\text{A3})$$

$$\tilde{\pi} = \frac{1}{1 + [\exp(\alpha_k + \beta_{kj} X_j)]_k}, \quad (\text{A4})$$

with $k = 1, \dots, n - 1$ a summation index. The reference category is arbitrary, and thus it was chosen to be the last one: $\tilde{\pi} = \pi_n$. The MATLAB implementation of the maximum likelihood estimator was used to determine the coefficients β_{ij} for this model (via the `mnrfit` function).

REFERENCES

- Almeira, G. J., and B. Scian, 2006: Some atmospheric and oceanic indices as predictors of seasonal rainfall in the Del Plata Basin of Argentina. *J. Hydrol.*, **329**, 350–359, doi:10.1016/j.jhydrol.2006.02.027.
- Barnston, A. G., and H. M. van den Dool, 1993: A degeneracy in cross-validated skill in regression-based forecasts. *J. Climate*, **6**, 963–977, doi:10.1175/1520-0442(1993)006<0963:ADICVS>2.0.CO;2.
- Barreiro, M., and A. Tippmann, 2008: Atlantic modulation of El Niño influence on summertime rainfall over southeastern South America. *Geophys. Res. Lett.*, **35**, L16704, doi:10.1029/2008GL035019.
- Barros, V. R., and G. E. Silvestri, 2002: The relation between sea surface temperature at the subtropical south-central Pacific and precipitation in southeastern South America. *J. Climate*, **15**, 251–267, doi:10.1175/1520-0442(2002)015<0251:TRBSST>2.0.CO;2.
- Bettolli, M. L., W. M. Vargas, and O. C. Penalba, 2009: Soya bean yield variability in the Argentine Pampas in relation to synoptic weather types: Monitoring implications. *Meteor. Appl.*, **16**, 501–511, doi:10.1002/met.148.
- Braman, L. M., M. K. van Aalst, S. J. Mason, P. Suarez, Y. Ait-Chellouche, and A. Tall, 2013: Climate forecasts in disaster management: Red Cross flood operations in West Africa, 2008. *Disasters*, **37**, 144–164, doi:10.1111/j.1467-7717.2012.01297.x.
- Cazes-Boezio, G., A. W. Robertson, and C. R. Mechoso, 2003: Seasonal dependence of ENSO teleconnections over South America and relationships with precipitation in Uruguay. *J. Climate*, **16**, 1159–1176, doi:10.1175/1520-0442(2003)16<1159:SDOETO>2.0.CO;2.
- Chan, S. C., S. K. Behera, and T. Yamagata, 2008: Indian Ocean dipole influence on South American rainfall. *Geophys. Res. Lett.*, **35**, L14S12, doi:10.1029/2008GL034204.
- Chen, M., W. Shi, P. Xie, V. B. S. Silva, V. E. Kousky, R. Wayne Higgins, and J. E. Janowiak, 2008: Assessing objective techniques for gauge-based analyses of global daily precipitation. *J. Geophys. Res.*, **113**, D04110, doi:10.1029/2007JD009132.
- Diaz, A. F., C. D. Studzinski, and C. R. Mechoso, 1998: Relationships between precipitation anomalies in Uruguay and southern Brazil and sea surface temperature in the Pacific and Atlantic Oceans. *J. Climate*, **11**, 251–271, doi:10.1175/1520-0442(1998)011<0251:RBPAIU>2.0.CO;2.
- Drumond, A. R. M., and T. Ambrizzi, 2008: The role of the south Indian and Pacific Oceans in South American monsoon variability. *Theor. Appl. Climatol.*, **94**, 125–137, doi:10.1007/s00704-007-0358-5.
- Goddard, L., W. E. Baethgen, H. Bhojwani, and A. W. Robertson, 2014: The International Research Institute for Climate & Society: Why, what and how. *Earth Perspect.*, **1**, 10, doi:10.1186/2194-6434-1-10.
- Grimm, A. M., 2003: The El Niño impact on the summer monsoon in Brazil: Regional processes versus remote influences. *J. Climate*, **16**, 263–280, doi:10.1175/1520-0442(2003)016<0263:TENIOT>2.0.CO;2.
- , S. E. T. Ferraz, and J. Gomes, 1998: Precipitation anomalies in southern Brazil associated with El Niño and La Niña events. *J. Climate*, **11**, 2863–2880, doi:10.1175/1520-0442(1998)011<2863:PAISBA>2.0.CO;2.
- , V. R. Barros, and M. E. Doyle, 2000: Climate variability in southern South America associated with El Niño and La Niña events. *J. Climate*, **13**, 35–58, doi:10.1175/1520-0442(2000)013<0035:CVISSA>2.0.CO;2.
- , J. S. Pal, and F. Giorgi, 2007: Connection between spring conditions and peak summer monsoon rainfall in South America: Role of soil moisture, surface temperature, and topography in eastern Brazil. *J. Climate*, **20**, 5929–5945, doi:10.1175/2007JCLI1684.1.
- Hirata, F. E., and A. M. Grimm, 2016: The role of synoptic and intraseasonal anomalies in the life cycle of summer rainfall extremes over South America. *Climate Dyn.*, **46**, 3041–3055, doi:10.1007/s00382-015-2751-6.
- Hoskins, B. J., 2013: The potential for skill across the range of the seamless weather-climate prediction problem: A stimulus for our science. *Quart. J. Roy. Meteor. Soc.*, **139**, 573–584, doi:10.1002/qj.1991.
- Huth, R., C. Beck, and O. E. Tveito, 2010: Preface. *Phys. Chem. Earth*, **35**, 307–308, doi:10.1016/j.pce.2010.06.005.
- Jolliffe, I., and A. Philipp, 2010: Some recent developments in cluster analysis. *Phys. Chem. Earth*, **35**, 309–315, doi:10.1016/j.pce.2009.07.014.
- , and D. Stephenson, Eds., 2012: *Forecast Verification: A Practitioner's Guide in Atmospheric Science*. 2nd ed. Wiley and Sons, 292 pp.

- Kalnay, E., and Coauthors, 1996: The NCEP/NCAR 40-Year Reanalysis Project. *Bull. Amer. Meteor. Soc.*, **77**, 437–471, doi:10.1175/1520-0477(1996)077<0437:TNYRP>2.0.CO;2.
- Kistler, R., and Coauthors, 1999: The NCEP–NCAR 50-Year Reanalysis: Monthly means CD-ROM and documentation. *Bull. Amer. Meteor. Soc.*, **82**, 247–267, doi:10.1175/1520-0477(2001)082<0247:TNNYRM>2.3.CO;2.
- Krishnamurthy, V., and J. Shukla, 2008: Seasonal persistence and propagation of intraseasonal patterns over the Indian monsoon region. *Climate Dyn.*, **30**, 353–369, doi:10.1007/s00382-007-0300-7.
- Li, S., and A. W. Robertson, 2015: Evaluation of submonthly precipitation forecast skill from global ensemble prediction systems. *Mon. Wea. Rev.*, **143**, 2871–2889, doi:10.1175/MWR-D-14-00277.1.
- Lorenz, E. N., 1969: Atmospheric predictability as revealed by naturally occurring analogues. *J. Atmos. Sci.*, **26**, 636–646, doi:10.1175/1520-0469(1969)26<636:APARBN>2.0.CO;2.
- Mason, S. J., and O. Baddour, 2008: Statistical modelling. *Seasonal Climate: Forecasting and Managing Risk*, A. Troccoli et al., Eds., NATO Science Series: IV, Vol. 82, Springer, 163–201.
- , and D. Stephenson, 2008: How do we know whether seasonal climate forecasts are any good? *Seasonal Climate: Forecasting and Managing Risk*, A. Troccoli et al., Eds., NATO Science Series: IV, Springer, 259–289.
- , and M. K. Tippett, 2016: Climate predictability tool version 15.3. International Research Institute for Climate and Society, doi:10.7916/D8NS0TQ6.
- , C. A. T. Ferro, and W. A. Landman, 2016: Forecasts of “normal.” *Quart. J. Roy. Meteor. Soc.*, in press.
- Mechoso, C. R., and Coauthors, 2001: Climatology and hydrology of La Plata Basin. VAMOS Scientific Study Group on the Plata Basin Tech. Rep., 56 pp. [Available online at http://www.atmos.umd.edu/~berbery/lpb/science_plan.html.]
- Moron, V., A. W. Robertson, M. N. Ward, and O. Ndiaye, 2010: Weather types and rainfall over Senegal. Part II: Downscaling of GCM simulations. *J. Climate*, **21**, 288–307, doi:10.1175/2007JCLI1624.1.
- , —, and M. Ghil, 2012: Impact of the modulated annual cycle and intraseasonal oscillation on daily-to-interannual rainfall variability across monsoonal India. *Climate Dyn.*, **38**, 2409–2435, doi:10.1007/s00382-011-1253-4.
- , P. Camberlin, and A. W. Robertson, 2013: Extracting subseasonal scenarios: An alternative method to analyze seasonal predictability of regional-scale tropical rainfall. *J. Climate*, **26**, 2580–2600, doi:10.1175/JCLI-D-12-00357.1.
- , A. W. Robertson, J.-H. Qian, and M. Ghil, 2015: Weather types across the Maritime Continent: From the diurnal cycle to interannual variations. *Front. Environ. Sci.*, **2**, doi:10.3389/fenvs.2014.00065.
- Muñoz, A., and L. Goddard, 2014: Multi-decadal climate information for agricultural planning in southeastern South America. *Extended Abstracts, 14th EMS Annual Meeting*, Prague, Czech Republic, European Meteorological Society, EMS2014-593.
- , —, A. W. Robertson, Y. Kushnir, and W. Baethgen, 2015: Cross-time scale interactions and rainfall extreme events in southeastern South America for the austral summer. Part I: Potential predictors. *J. Climate*, **28**, 7894–7913, doi:10.1175/JCLI-D-14-00693.1.
- Nogués-Paegle, J., and K. C. Mo, 1997: Alternating wet and dry conditions over South America during summer. *Mon. Wea. Rev.*, **125**, 279–291, doi:10.1175/1520-0493(1997)125<0279:AWADCO>2.0.CO;2.
- Palmer, T., 1999: A nonlinear dynamical perspective on climate prediction. *J. Climate*, **12**, 575–591, doi:10.1175/1520-0442(1999)012<0575:ANDPOC>2.0.CO;2.
- Park, H.-S., and C.-H. Jun, 2009: A simple and fast algorithm for K-medoids clustering. *Expert Syst. Appl.*, **36**, 3336–3341, doi:10.1016/j.eswa.2008.01.039.
- Pisciottano, G., A. Díaz, G. Cazess, and C. R. Mechoso, 1994: El Niño–Southern Oscillation impact on rainfall in Uruguay. *J. Climate*, **7**, 1286–1302, doi:10.1175/1520-0442(1994)007<1286:ENSOIO>2.0.CO;2.
- Saha, S., and P. Tripp, 2011: CFSv2 retrospective forecasts. NOAA/NWS/NCEP Environmental Modeling Center Tech. Rep., 12 pp.
- , and Coauthors, 2014: The NCEP Climate Forecast System version 2. *J. Climate*, **27**, 2185–2208, doi:10.1175/JCLI-D-12-00823.1.
- Smith, T. M., R. W. Reynolds, T. C. Peterson, and J. Lawrimore, 2008: Improvements to NOAA’s historical merged land–ocean surface temperature analysis (1880–2006). *J. Climate*, **21**, 2283–2296, doi:10.1175/2007JCLI2100.1.
- Van den Dool, H. M., 1994: Searching for analogues, how long must we wait? *Tellus*, **46A**, 314–324, doi:10.3402/tellusa.v46i3.15481.
- Vitart, F., 2014: Evolution of ECMWF sub-seasonal forecast skill scores. *Quart. J. Roy. Meteor. Soc.*, **140**, 1889–1899, doi:10.1002/qj.2256.
- Wheeler, M. C., and H. H. Hendon, 2004: An all-season real-time multivariate MJO index: Development of an index for monitoring and prediction. *Mon. Wea. Rev.*, **132**, 1917–1932, doi:10.1175/1520-0493(2004)132<1917:AARMMI>2.0.CO;2.
- WMO, 2013: Subseasonal to seasonal prediction: Research implementation plan. WMO Tech. Rep., 63 pp.
- Yoo, J. H., A. W. Robertson, and I.-S. Kang, 2010: Analysis of intraseasonal and interannual variability of the Asian summer monsoon using a hidden Markov model. *J. Climate*, **23**, 5498–5516, doi:10.1175/2010JCLI3473.1.
- Zorita, E., and H. von Storch, 1999: The analog method as a simple statistical downscaling technique: Comparison with more complicated methods. *J. Climate*, **12**, 2474–2489, doi:10.1175/1520-0442(1999)012<2474:TAMAAS>2.0.CO;2.